**Article:**
Wang, C., Lv, G., Li, Y. et al. (2 more authors) (2024) Selective catalytic reduction of NOX with $CH_4$ over In/SSZ-13 zeolites: The enhancement of high-temperature catalytic activity by Ce modification. Journal of Environmental Chemical Engineering, 12 (1). 111830. ISSN 2213-2929

https://doi.org/10.1016/j.jece.2023.111830

# Selective catalytic reduction of $NO_X$ with $CH_4$ over In/SSZ-13 zeolites: the enhancement of high-temperature catalytic activity by Ce modification

Chenxi Wang, Gang Lv, Yunqiang Li, Ye Liu, Chonglin Song*

State Key Laboratory of Engines, Tianjin University, Tianjin 300072, China

*Corresponding author:

Chonglin Song, State Key Laboratory of Engines, Tianjin University, Tianjin, China

Fax: +86-22-27403750; Tel.: +86-22-27406840-8020

Email address: songchonglin@tju.edu.cn (C.L. Song)

## Abstract

The selective catalytic reduction of nitrogen oxides by methane ($CH_4$/$NO_X$-SCR) is a potential technique for the abatement of the $NO_X$ emissions from lean-burn GDI engines, due to the excellent thermal stability of $CH_4$. This work focuses on the promotion of In/SSZ-13 catalysts by Ce modification for the $CH_4$/$NO_X$-SCR performance at high temperatures. A series of In/SSZ-13 and Ce-In/SSZ-13 catalysts were prepared using the wetness impregnation method. The effects of Ce modification on the catalytic performance were analysed in detail using the scanning electron microscopy, X-ray diffraction, X-ray photoelectron spectroscopy, ultraviolet-visible diffuse reflectance spectrum and temperature-programmed desorption/reduction techniques. The results show that the Ce modification significantly enhances the high-temperature activity of the In/SSZ-13 catalysts for the $NO_X$-SCR reaction, especially for the 5 wt.% Ce-15 wt.% In/SSZ-13 sample which

has more than 75% $NO_X$ conversion at 390-700°C. In addition, the Ce modification enhances the water vapor tolerance of the catalyst sample. The Ce modification increases not only the concentration of surface chemisorption oxygen species, but also the relative amount of $InO^+$ species which serve as the main active sites for $CH_4$ activation. Furthermore, the incorporation of Ce into In/SSZ-13 greatly promotes $NO_X$ adsorption on the catalyst surface. Most importantly, the Ce modification makes In species well-dispersed on the catalyst surface and thus suppresses the formation of bulk $In_2O_3$ species which are more active for the $CH_4$ non-selective oxidation. The combination of all these effects results in the Ce-In/SSZ-13 samples with the superior catalytic activity.

**Keywords:** Selective catalytic reduction; Nitrogen oxides; Methane; In/SSZ-13 catalyst; Ce modification; Non-selective oxidation

## 1. Introduction

Carbon dioxide ($CO_2$) emission has become a great concern throughout the entire world due to its significant contribution to global warming. For vehicle engines, high thermal efficiency combustion modes with low-fuel consumption are the most effective solution to reduce $CO_2$ emissions. Compared with the traditional stoichiometry combustion in gasoline direct injection (GDI) engines, the lean-burn mode can achieve lower combustion temperature due to excess oxygen ($O_2$) under similar operating conditions. Thus, higher thermal efficiency and lower fuel consumption can be achieved by further increasing compression ratio or advancing ignition timing, and as a consequence, significantly reduce $CO_2$ emissions [1][2][3]. Nevertheless, the lean-burn mode produces excess $O_2$ in the engine exhaust stream, invalidating the $NO_X$ removal ability of traditional three-way catalytic systems [4][5]. Therefore, the efficient removal of exhaust nitrogen oxides ($NO_X$) is the major obstacle to practical application of the lean-burn mode in GDI engines.

At present, selective catalytic reduction (SCR) of NOx with ammonia ($NH_3$) has been commercialized in diesel engines to efficiently reduce $NO_X$ in the oxygen-rich exhaust gas [6][7]. For the $NH_3$/$NO_X$-SCR technology, however, non-selective oxidation of $NH_3$ will occur concurrently with $NO_X$ SCR reaction approximately at the reaction temperatures above 400°C [8][9], which results in a decrease in $NO_X$ conversion and $N_2O$ generation [10]. Lean-burn GDI engines usually have exhaust temperatures of 500-700°C under normal operating conditions [11][12]. Such high exhaust temperatures inevitably cause a severe $NH_3$ oxidation, and so the SCR technology based on $NH_3$ as reductant is unsuitable for the $NO_X$ abatement of lean-burn GDI engines.

Methane ($CH_4$), a simplest hydrocarbon in structure, has excellent thermal stability at high temperatures because of its high C-H bond dissociation energy (439 kJ/mol) [13][14][15]. Moreover, $CH_4$ also possesses non-toxic, non-corrosive, easily-available and low-cost characteristics. These merits highlight that $CH_4$ is a promising SCR reductant for the high-temperature $NO_X$ removal in lean-burn GDI engines. Since Li and Armor et al. [16] discovered that Co/ZSM-5 zeolite has an excellent performance in catalyzing $CH_4$ to reduce $NO_X$, numerous metal-modified zeolite catalysts have been proposed for the $CH_4/NO_X$-SCR reaction. Table 1 summarizes some representative studies on the zeolite catalysts used for $CH_4/NO_X$-SCR [17-24]. It can be seen that the maximum $NO_X$ conversions of most catalysts occur above 500°C, indicating that the $CH_4/NO_X$-SCR has an excellent high-temperature catalytic activity as compared to the $NH_3/NO_X$-SCR. In addition, Indium (In)-modified zeolites demonstrate a remarkable $CH_4/NO_X$-SCR performance at high temperatures. For example, Pan et al. [17] discovered that the H-BEA zeolite with 4 wt.% In modification could achieve 97% $NO_X$ conversion at 550°C. The high activity of In is attributed to the O site in the $InO^+$ species which is an excellent active site to promote C-H bond cleavage, which significantly promotes the activation of $CH_4$ and favors the SCR reaction [25]. However, it is difficult to further enhance the high-temperature activity of the catalysts simply by increasing In content because excessive In loading will inevitably lead to the formation of large $In_2O_3$ particles, which facilitate the non-selective oxidation of $CH_4$ that decreases $NO_X$ conversions at high temperatures [25][26]. An alternative is to introduce a second transition metal to In/SSZ-13 catalysts. Cerium (Ce) is a good potential candidate for increasing zeolite activity due to its excellent abilities in facilitating oxygen store,

zeolites defect sites covering and metal dispersion [27][28]. Sowade et al. [22] found that the high NO oxidation activity of Ce provided a sufficient $NO_2$ supply in SCR reaction, and thus favored the SCR reaction. Li et al. [23] reported that the incorporation of Ce into metal-modified zeolites stabilized metal ions and improved the hydrothermal stability of Ag/ZSM-5 catalyst.

**Table 1** Some representative studies on the $CH_4/NO_X$-SCR zeolite catalysts

| Samples | Reaction conditions | Temperature | Max. $NO_X$ conversion |
|---|---|---|---|
| In/BEA [17] | 600 ppm NO, 25 ppm $NO_2$, 600 ppm $CH_4$, 6% $O_2$, $N_2$ balance, GHSV 18400 $h^{-1}$ | 350-550°C | 97% at 550°C |
| Mn/Beta [18] | 2180 ppm NO, 2050 ppm $CH_4$, 2% $O_2$, 5% $H_2O$, He balance, GHSV 7500 $h^{-1}$ | 300-600°C | 61% at 500°C |
| Fe/BEA [19] | 1000 ppm NO, 2000 ppm $CH_4$, 2% $O_2$, He balance, GHSV 10000 $h^{-1}$ | 250-500°C | 23% at 400°C |
| Co/ZSM-5 [20] | 1000 ppm NO, 5000 ppm $CH_4$, 2% $O_2$, He balance, GHSV 6000 $h^{-1}$ | 300-600°C | 98% at 500°C |
| Ag/ZSM-5 [20] | 1000 ppm NO, 5000 ppm $CH_4$, 2% $O_2$, He balance, GHSV 6000 $h^{-1}$ | 300-600°C | 63% at 550°C |
| Pd/HMOR [21] | 1000 ppm NO, 1000 ppm $CH_4$, 7% $O_2$, He balance, GHSV 40000 $h^{-1}$ | 250-500°C | 25% at 500°C |
| Ce-Pd/HMOR [21] | 1000 ppm NO, 1000 ppm $CH_4$, 7% $O_2$, Ar balance, GHSV 40000 $h^{-1}$ | 300-500°C | 34% at 500°C |
| CeOx-In/ZSM-5 [22] | 1000 ppm NO, 1000 ppm $CH_4$, 2% $O_2$, He balance, GHSV 30000 $h^{-1}$ | 350-550°C | 92% at 500°C |
| Ce-Ag/ZSM-5 [23] | 5000 ppm NO, 5000 ppm $CH_4$, 2.5% $O_2$, He balance, GHSV 7500 $h^{-1}$ | 450-600°C | 80% at 500°C |

At present, the researches on the $CH_4/NO_X$-SCR catalysts focused mostly on the $NO_X$ reduction performance in the temperature range of 200-600°C and low-temperature activity, aiming to reduce the $NO_x$ emissions from diesel engines or power plants with exhaust below 550°C. Considering the negative effects of $CH_4$ non-selective oxidation on the $CH_4/NO_X$-SCR performance at the high temperatures above 600°C, the current catalysts cannot be directly applied in lean-burn GDI engines which have the exhaust temperature of 500-700°C. However, highly efficient $CH_4/NO_X$-SCR catalysts available for lean-burn GDI

engines were rarely reported, and thus it is essential to perform comprehensive studies on this issue. Moreover, the promotional mechanism of catalyst modification on the $CH_4/NO_X$-SCR performance at high temperatures is required for further understanding.

The aim of the present work was to develop a $CH_4/NO_X$-SCR catalyst that has great potential for NOx abatement of lean-burn GDI engines. Given the superior hydrothermal stability against framework dealumination of chabazite (CHA) structured small-pore H-SSZ-13 zeolite [29][30], Ce modified In/SSZ-13 $CH_4/NO_X$-SCR catalysts were used for this purpose. According to the actual exhaust temperatures of lean-burn GDI engines, the $CH_4/NO_X$-SCR performance was evaluated in the temperature range of 200-700°C. The changes of structure, surface chemical states composition, reducibility, acid sites, $NO_X$ adsorption and $CH_4$ utilization efficiency (CUE) after the Ce modification were explored. In addition, the promoting mechanism of Ce modification on high-temperature catalytic activity over In-modified catalyst was discussed in detail.

## 2. Experimental Setup

### *2.1. Catalyst preparation*

A H-SSZ-13 zeolite (Zhuoran Environmental Protection Co., Ltd) with a Si/Al ratio of 30 was employed as the support to prepare the modified catalysts. In and Ce were modified on H-SSZ-13 zeolite via the wetness impregnation method. Specifically, a desired quantity of $In(NO_3)_3$ and $In(NO_3)_3$+$Ce(NO_3)_3$ (Aladdin Biochemical Technology Co., Ltd) was dissolved in 100 mL distilled water respectively to form aqueous solutions for monometallic and bimetallic modification. A total of 5 g H-SSZ-13 zeolite was suspendered in the above aqueous solutions, in which the pH values were adjusted to 2 by adding $HNO_3$. After stirring

for 5 h at 70°C in a thermostatic stirrer, the water in the solution was removed at 70°C. The obtained solid residues were dried at 110°C for 5 h, then calcined in a muffle furnace at 700°C for 4 h. The In contents in In/SSZ-13 series samples of 5, 10, 15, and 20 wt.%, and second promoting metal Ce contents of 1, 5, and 10 wt.% were employed in this study. The resulting catalyst samples were designated as *a*% Ce-*b*% In/SSZ-13, where *a* and *b* represented the weight contents of the Ce and In elements, respectively.

*2.2. Catalytic performance*

Catalytic activity tests were conducted in a vertical fixed-bed quartz tube reactor at atmosphere pressure. Several K-type thermocouples and PID-controlled furnaces were used to adjust the target temperatures, and the gas flow rates were controlled by mass flow controllers. A total of 1.5 mL catalyst sample (20-40 mesh) was loaded into the reactor with an inner diameter of 7 mm. The feed gas was composed of 1000 ppm NO, 3000 ppm $CH_4$, 8 vol % $O_2$, 5 vol% water vapor (only used for the water vapor tolerance test) and balance Ar with a GHSV of 30000 $h^{-1}$. Before the measurement, the catalysts were pretreated by Ar at a flow rate of 1000 mL $min^{-1}$ at 400°C for 1 h, and then cooled down to 200°C. In the NO oxidation test, the NO oxidation ability of the catalysts was examined using the feed gas consisting of 1000 ppm NO, 8 vol% $O_2$ and balance Ar with a GHSV of 30000 $h^{-1}$. During tests, the steady-state outlet compositions were measured by an on-line mass spectrometer (V&F, AS-021). The key parameters for evaluating the catalytic performance are defined as follows:

$$NO_x\ conversion = \frac{C_{NO_x(in)} - C_{NO_x(out)}}{C_{NO_x(in)}} \times 100\% \quad (1)$$

$$CH_4\ conversion = \frac{C_{CH_4(in)} - C_{CH_4(out)}}{C_{CH_4(in)}} \times 100\% \quad (2)$$

$$NO\ to\ NO_2\ conversion = \frac{C_{NO_2(out)}}{C_{NO_x(in)}} \times 100\% \quad (3)$$

where $C_{NOx(in)}$, $C_{NOx(out)}$, $C_{CH4(in)}$ and $C_{CH4(out)}$ are the concentrations of $NO_X$ and $CH_4$ at the reactor inlet and outlet, respectively. $C_{NO2(out)}$ is the $NO_2$ concentration at the reactor outlet. To analyse the $CH_4$ non-selective oxidation in $CH_4/NO_X$-SCR process, $CH_4$ utilization efficiency (CUE) was evaluated for the catalyst samples. Here, CUE refers to the ratio of the $CH_4$ involved in SCR reaction to the total $CH_4$ consumed during trials. The CUE is calculated according to the following equation:

$$CUE = \frac{C_{NOx(in)} - C_{NOx(out)}}{2 \times (C_{CH_4(in)} - C_{CH_4(out)})} \times 100\% \quad (4)$$

where the constant 2 in Eq. (4) is the stoichiometric ratio of NO to $CH_4$ in $CH_4/NO_X$-SCR reaction as shown in Eq. (5) [31][32].

$$2NO + CH_4 + O_2 \rightarrow N_2 + CO_2 + 2H_2O \quad (5)$$

*2.3. Catalyst characterization*

The weight contents of In and Ce in the catalyst samples were verified using an inductively coupled plasma optical emission spectroscopy (ICP-OES, Thermofisher, iCAP 7200). The catalyst morphology was recorded by a scanning electron microscopy (SEM, FEI-Verios 460 L). The element mapping analysis was performed using a coupled energy dispersive X-ray spectroscopy detector (EDX). The X-ray diffraction (XRD, Rigaku Smart Lab) spectra of the catalyst samples were measured by a powder diffractometer with a Cu-Kα source (40 kV, λ=1.5406 Å). The scanning rate was 8 °/min and the spectra were recorded from 5 to 80°. The unit cell parameters were obtained through analysing the

diffraction patterns using Pawley refinement in Material Studio software [33]. Ultraviolet-visible diffuse reflectance spectra (UV-vis DR, Shimadzu UV-2600) were measured on a UV-vis spectrophotometer. Powder samples were measured by integration sphere diffuse reflectance technique at room temperature, and the wavelength scanning range is from 200 to 800 nm. The X-ray photoelectron spectra (XPS, Kratos Analytical, Axis Supra) of the catalyst samples were obtained using a spectrometer with Al-Kα source. Prior to analysis, the accurate binding energies were corrected by referring to the C1s peak at 284.8 eV.

The NO, NO+$O_2$ and $NH_3$ temperature-programmed desorption (NO-TPD, NO+$O_2$-TPD and $NH_3$-TPD) tests were conducted on a Pulsar analyzer (Quantachrome ChemBet). In tests, 60 mg sample with 40-60 mesh was used to evaluate catalyst adsorption ability. Before the test, the catalyst samples were pretreated in a flow of Ar at 400°C for 30 min. Then, the samples were cooled down by flowing Ar, and the feeding gases, including 1% NO+99% Ar, 1% NO+10% $O_2$+89% Ar and 1% $NH_3$+99% Ar, were fed into the reactor. After saturated adsorption NO or NO+$O_2$ or $NH_3$, the Ar with 60 mL/min was fed for 30 min to remove weakly adsorption species on catalysts. Then, the desorption product intensities were recorded from 50-700°C with a heating rate of 10°C/min. The intensity profiles were recorded by an on-line mass spectrometer (Ametek, LC-D200). The amount of desorption products was calculated by integration program according to the intensity profiles. The $H_2$ temperature-programmed reduction ($H_2$-TPR) test was also conducted on the Pulsar analyzer. The feeding gas of 5% $H_2$+95% Ar was fed into the reactor with 60 mL/min, and the $H_2$ intensity profiles were record from 50-700°C at a heating rate of 10°C/min.

## 3. Results and discussion

### *3.1. Catalytic performance*

The modified metal contents were analyzed by the ICP-OES and listed in Table 2. The weight contents of In and Ce in all the samples are consistent with the experimental design goals.

**Table 2** The elemental content analysis of catalyst samples

| Samples | In content (wt.%) | Ce content (wt.%) |
|---|---|---|
| 5% In/SSZ-13 | 4.4 | - |
| 10% In/SSZ-13 | 9.7 | - |
| 15% In/SSZ-13 | 14.8 | - |
| 20% In/SSZ-13 | 19.3 | - |
| 1% Ce-15% In/SSZ-13 | 14.7 | 1.1 |
| 5% Ce-15% In/SSZ-13 | 14.6 | 4.6 |
| 10% Ce-15% In/SSZ-13 | 14.4 | 9.5 |

Figures 1 and 2 show the temperature-dependent conversions of $NO_X$ and $CH_4$ over the In/SSZ-13 and Ce-In/SSZ-13 series catalysts. It is seen from Fig. 1(a) that the catalyst samples have an increase in the $NO_X$ conversion with increasing the In loading from 5% to 15%, indicative of an improvement of the catalytic activity. However, as the In loading further increases from 15% to 20%, no significant increase in the $NO_X$ conversion are found, and even there is an considerable decrease at of 600-700°C temperature range. At the same time, the $CH_4$ conversions in Fig. 1(b) increase in response to increases in the reaction temperature and In loading. Given the decrease in the $NO_X$ conversion above 550°C, as indicated in Fig. 1(a), it is confirmed that the increased $CH_4$ conversion in the high-temperature region is primarily due to the non-selective oxidation of $CH_4$ with $O_2$.

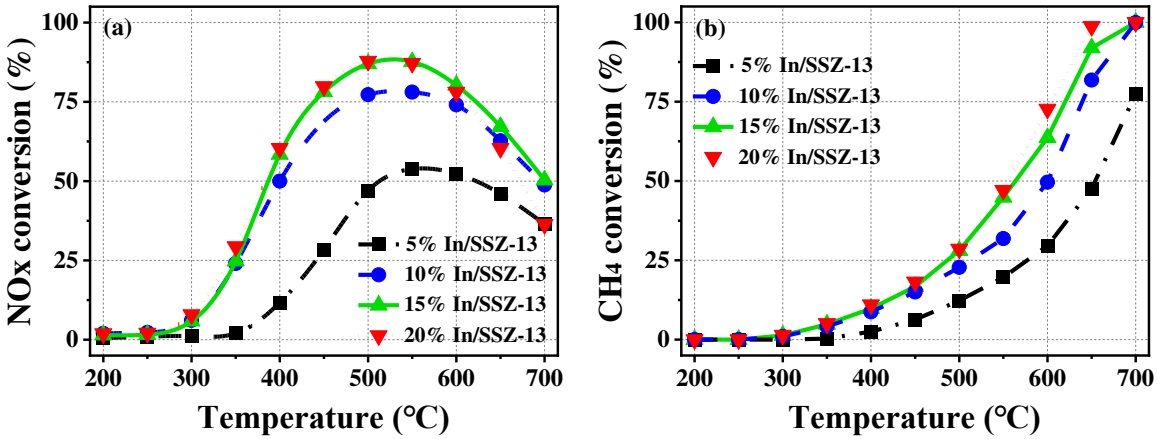


**Fig. 1.** $CH_4/NO_X$-SCR performance over the In/SSZ-13 series catalysts.

Among the In/SSZ-13 series catalysts, the 15% In/SSZ-13 catalyst exhibits the best catalytic performance, with the maximum $NO_X$ conversion of 87.6% at 550°C and a $NO_X$ conversion of >75% in the temperature range of 440-620°C. Therefore, this catalyst was employed to perform the modification of In/SSZ-13 catalyst with Ce so as to further improve the catalytic performance. Figure 2 presents the $NO_X$ and $CH_4$ conversions as a function of temperature over the Ce-15% In/SSZ-13 series catalysts. After Ce modification, almost no change in the $NO_X$ conversion is observed below 350°C. However, there is a significant promotion in the $NO_X$ conversion at high-temperature region of 400-700°C. For example, the 5% Ce-15% In/SSZ-13 catalyst has more than 75% $NO_X$ conversion at 390-700°C and almost 100% $NO_X$ conversion at 450-620°C. Similar to the In/SSZ-13 series catalysts, the Ce-15% In/SSZ-13 series catalysts also demonstrate an increase in the $CH_4$ conversion with the increases in reaction temperature and Ce loading, as indicated in Fig. 2(b).

Several literatures have reported the $CH_4/NO_X$-SCR activity of zeolite-based catalysts with bimetallic modification under the reaction conditions similar to those in this study.

Mendes et al. [21] found that the Pd-Ce/HMOR catalyst after modification only reached 34% $NO_X$ conversion at 500°C. Sowade et al. [22] asserted that the Ce-In/ZSM-5 catalysts exhibited a maximum $NO_X$ conversion of 90% at 500°C and the 75% conversion at 380-560°C. In the studies of Yang et al. [26][34], the Cr-In/SSZ-13 and Ru-In/SSZ-13 catalysts were discovered to have 75% $NO_X$ conversion at 490-550°C and 450-550°C, respectively. In the present work, the In and Ce modification greatly promotes the catalytic activity of the H-SSZ-13 catalyst, especially in the temperature region of 450-620°C where approximately 100% $NO_X$ conversion is achieved. Given that the 5% Ce-15% In/SSZ-13 catalyst possesses the best catalytic performance among the Ce-15% In/SSZ-13 series catalysts, it was used to explain the promotional effects of Ce modification on the $CH_4/NO_X$-SCR.

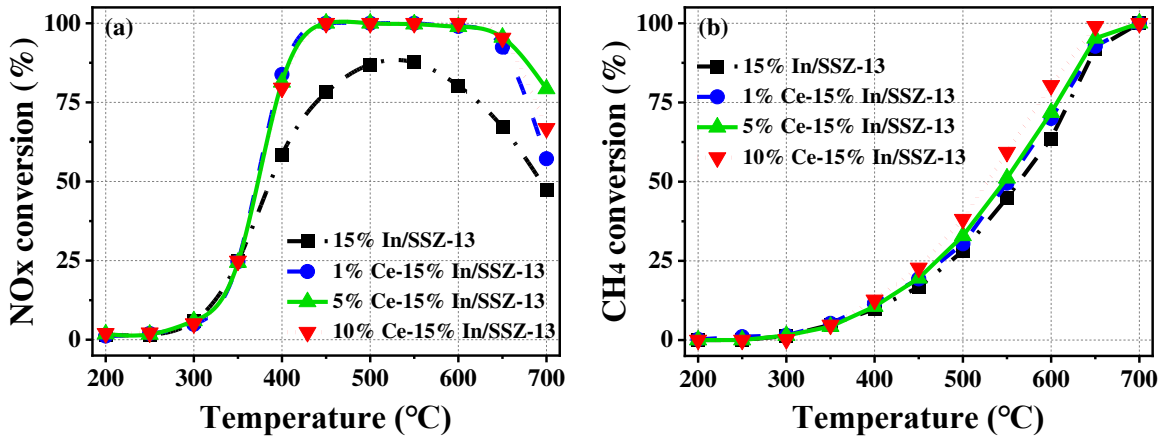


**Fig. 2.** $CH_4/NO_X$-SCR performance over the 15% In/SSZ-13 catalysts with various Ce loading.

*3.2. Water vapor tolerance*

In the lean-burn GDI engine exhaust, $H_2O$ is a non-negligible factor affecting the SCR reaction, because the competitive adsorption of $H_2O$ and reactants ($NO_X$ or $CH_4$) at the same active sites may results in a decrease of activity [35][36]. Figure 3 shows the influence of

water vapor on the activity of the 15% In/SSZ-13 and 5% Ce-15% In/SSZ-13 catalysts at 550°C, where the catalyst samples have the maximum $NO_X$ conversion as indicated in Fig. 2. Before adding water vapor, the catalyst samples were stabilized at 550°C for 60 min. Upon the introduction of 5 vol% water vapor into reactor, the $NO_X$ conversions first decrease from 87.6 to 69.3% for the 15% In/SSZ-13 catalyst and from 100 to 90.8% for the 5% Ce-15% In/SSZ-13 catalyst, and then remain almost unchanged. The marginal decrease in $NO_X$ conversion for the 5% Ce-15% In/SSZ-13 catalyst suggests that Ce modification increases the water vapor tolerance. After cutting off the introduction of water vapor, the $NO_X$ conversions for both catalyst samples gradually recover and reach the original level, indicating that the effect of water vapor on catalytic activity is reversible.

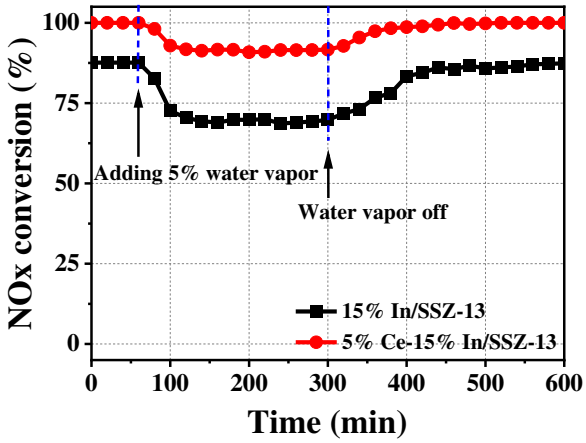


**Fig. 3.** Water vapor tolerance performance of the 15% In/SSZ-13 and 5% Ce-15% In/SSZ-13 catalysts.

### *3.3. Physicochemical characteristics*

#### *3.3.1. Morphology and structure*

Figure 4 presents the SEM images of the H-SSZ-13 and 5% Ce-15% In/SSZ-13 catalysts. The H-SSZ-13 catalyst displays typical zeolite particles with regular and smooth cubic structure [37]. For the 5% Ce-15% In/SSZ-13 catalyst, the basic cubic structure is remained, and some light spherical particles appear on the zeolite support surface. To identify the composition of these spherical particles, local EDX measurement was performed for Points 1-4 in Fig. 4. Due to the similarity in element composition of the spherical particles, only the element composition for Point 1 is shown in Fig. 4. It is obvious that the particles on the 5% Ce-15% In/SSZ-13 catalyst are mainly composed of O, Si, Al, In and Ce. The high contents of In, Ce and O elements highlights that the agglomeration of In-oxide and Ce-oxide species are formed on the zeolite surface. Figure 5 shows the element mapping images of the 5% Ce-15% In/SSZ-13 catalyst. It can be seen that the In (yellow spots) and Ce (red spots) species are uniformly dispersed and present close contact on the zeolite surface.

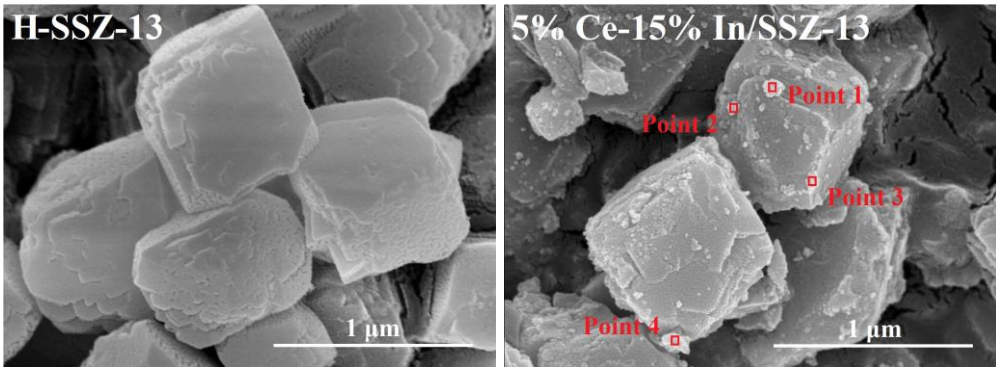

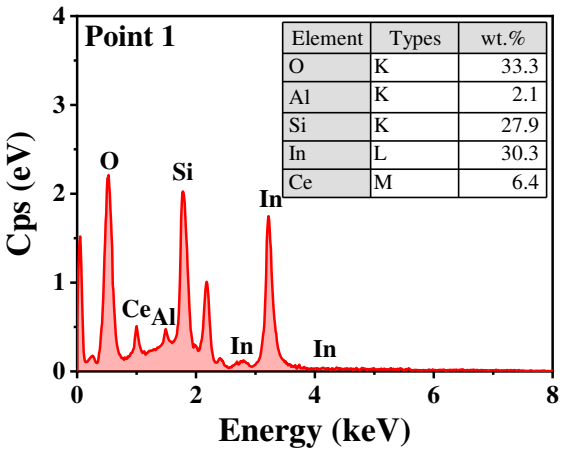


**Fig. 4.** SEM images and EDX analysis of the H-SSZ-13 and 5% Ce-15% In/SSZ-13 catalysts.

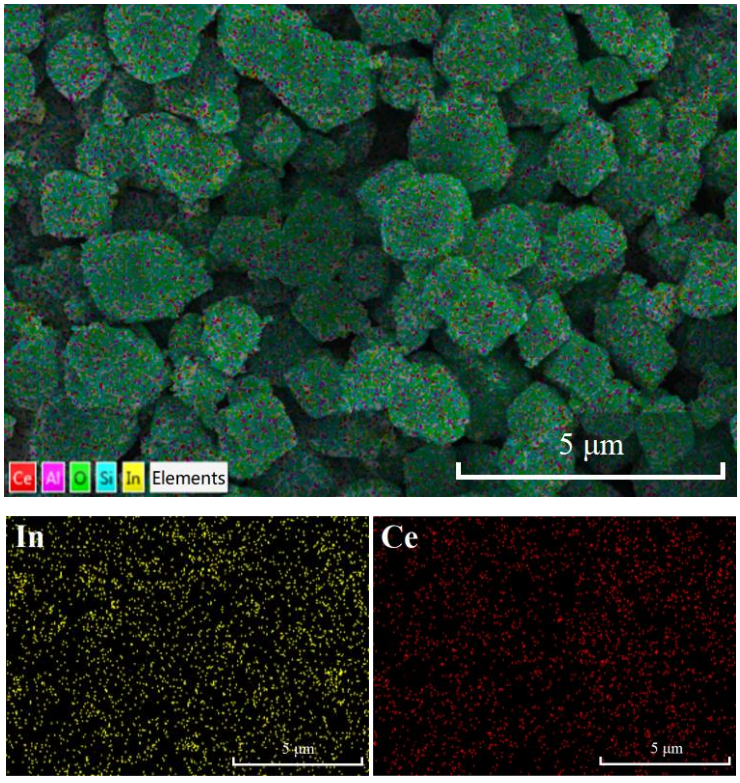


**Fig. 5.** Element mapping images of the 5% Ce-15% In/SSZ-13 catalysts.

Figure 6 presents the XRD spectra of the H-SSZ-13, 15% In/ SSZ-13 and 5% Ce-15% In/ SSZ-13 catalysts. All samples exhibit typical diffraction peaks of CHA topology (e.g. $2\theta$ =9.5°, 14.0°, 16.1°, 17.8°, 20.7°, and 25.0°), suggesting that the zeolite crystalline structure

is unchanged after modifying In and/or Ce. However, as compared to the H-SSZ-13 catalyst, the 15% In/SSZ-13 and 5% Ce-15% In/SSZ-13 catalysts exhibit a decrease in the intensity of the structure peaks as shown in Fig. 6(a), which illuminates that the In and Ce modification reduces the crystallinity and orderliness of zeolite [38]. Meanwhile, as listed in Table 3, the dimension of zeolite crystalline cell *a*-axis increases 0.06 and 0.08 Å after monometallic In and bimetallic Ce-In modification, respectively. This suggests that the In and Ce irons with large kinetic diameter achieve exchange with zeolite and enter into the cell interior [39].

In addition, the diffraction peaks of $In_2O_3$ species (PDF#71-2195) were found in partially enlarged image Fig. 6(b). Notably, the peak intensity for the 5% Ce-15% In/SSZ-13 catalyst is lower than that of the 15% In/SSZ-13 catalyst, which implies that the Ce modifying decreases the crystallinity and size of $In_2O_3$ species [40][41]. As shown in Table 3, to quantify the effects of Ce modification on $In_2O_3$ species size, the mean diameter *D* of the $In_2O_3$ crystalline on samples was obtained using Scherrer's equation [42]. Compared with In/SSZ-13 catalyst, the introduction of Ce leads to a decrease of 47% in the $In_2O_3$ mean diameter, indicating that Ce modification has an excellent dispersing effect on In species. Given that the promoting effect of large $In_2O_3$ cluster on $CH_4$ non-selective oxidation [25][26], the Ce modification may further increases CUE in $CH_4/NO_X$-SCR reaction. In Fig. 6, no obvious characteristic peaks belonging to $CeO_2$ (PDF#34-0394) are observed in the XRD spectra of the 5% Ce-15% In/ SSZ-13 catalyst. Thus, the Ce species are inferred to be well-dispersed on the zeolite surface so that their sizes are below the detection limit of the apparatus.

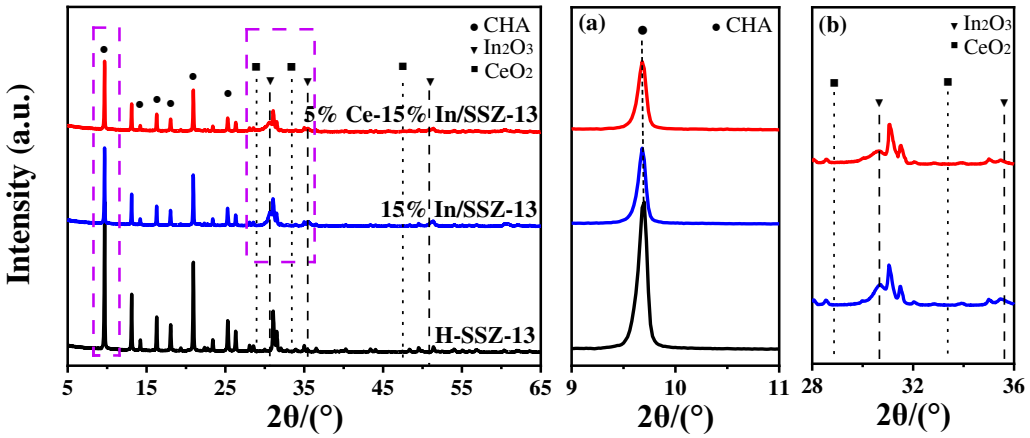


**Fig. 6.** XRD spectra of H-SSZ-13, 15% In/SSZ-13 and 5% Ce-15% In/SSZ-13 catalysts. (a) Partially enlarged image of 9-11◦; (b) Partially enlarged image of 28-36◦

**Table 3** Crystalline cell parameter (*a*) and $In_2O_3$ crystalline mean diameter (*D*)

| Samples | *a* (Å) | *D* (nm) |
|---|---|---|
| H-SSZ-13 | 9.18 | - |
| 15% In/SSZ-13 | 9.24 | 12.38 |
| 5% Ce-15% In/SSZ-13 | 9.26 | 6.54 |

*3.3.2. UV-vis DR analysis*

Figure 7 compares the UV-vis DR spectra of the H-SSZ-13, 15% In/SSZ-13 and 5% Ce-15% In/SSZ-13 catalysts. The spectrum of 15% In/SSZ-13 catalyst appears two absorption bands at about 220 nm and 310 nm, respectively. The 220 nm band corresponds to the radiative relaxation caused by the isolated In cations [43], which illuminates that a few In interact with acidic protons of zeolite to form exchanged In cations, indicating that some In achieves migration from zeolite exterior to interior [44]. The band at 310 nm is attributed to the radiative relaxation of the low-dimentional clusters In species on zeolite surface, which potentially associated with the bulk $In_2O_3$ [45]. For the 5% Ce-15% In/SSZ-13 catalyst, together with the bands at about 220 and 310 nm, two new absorption bands

appear at 260 and 290 nm. The band at 260 nm is assigned to the $Ce^{3+}$ in zeolite, and the 290 nm peak corresponds to the charge transfer from $O^{2-}$ to $Ce^{4+}$ in $CeO_2$ clusters [46][47]. The presence of the two new bands implies that the modified Ce is either incorporated into the framework of SSZ-13 zeolites or present in a highly dispersed $CeO_2$. In addition, close inspection of Fig. 7 shows that the band at 220 nm for the 5% Ce-15% In/SSZ-13 catalyst is slightly stronger than that for the 15% In/SSZ-13 catalyst, indicating that the Ce modification promotes the formation of isolated In-exchanged cations.

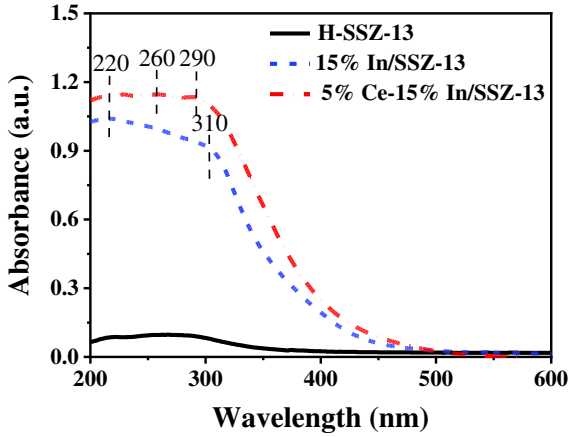


**Fig. 7.** UV-vis spectra of H-SSZ-13, 15% In/SSZ-13, and 5% Ce-15% In/SSZ-13 catalysts.

*3.3.3. XPS analysis*

XPS analysis was performed to further identify the chemical states and surface compositions of the catalysts. The XPS spectra of the 15% In/SSZ-13 and 5% Ce-15% In/SSZ-13 catalysts are plotted in Fig. 8. Following deconvolution of the XPS spectra, the surface compositions of the catalyst samples are determined and listed in Table 4. The In $3d_{5/2}$ spectra in Fig. 8(a) shows two peaks at 444.6 eV and 445.4 eV, which correspond to $In_2O_3$ and $InO^+$ species, respectively [48][49]. Here, $InO^+$ species are generally considered

the main active sites for $CH_4$ activation due to the strong activity of the O-p orbital of $InO^+$ to the C-p orbital of $CH_4$ [25][50]. It can be seen from Table 4 that the ratios of $InO^+/(InO^+ + In_2O_3)$ increase from 47.61% for the 15% In/SSZ-13 catalyst to 51.38% for the 5% Ce-15% In/SSZ-13 catalyst, consistent with the UV-vis results. This increase in the relative amount of $InO^+$ demonstrates that the Ce modification favors the generation of $InO^+$ species and thus provides more active sites for $CH_4$ activation. As a consequence, more active methyl groups are formed and improve the SCR reaction.

The O 1s spectra can be fitted into two peaks as shown in Fig. 8(b), which are assigned to the surface chemisorption oxygen species $O_a$ (the peak at 532 eV) and the lattice oxygen $O_\beta$ (the peak at 529.5 eV) [35][51]. As seen in Fig. 8(b), the Ce modification considerably increases the intensity of the $O_a$ peak. Table 4 indicates that the Ce modification results in a considerable increase in the ratio of $O_\alpha/(O_\alpha+O_\beta)$, from 72.2% for the 15% In/SSZ-13 catalyst to 82.2% for the 5% Ce-15% In/SSZ-13 catalyst. Because the $O_a$ has higher mobility than the $O_\beta$, the increase in the ratio of $O_\alpha/(O_\alpha+O_\beta)$ enhances the NO oxidation, which facilitates the $NO_X$ adsorption and reaction on catalyst surface [52][53].

The Ce 3d spectra in Fig. 8(c) manifests that $Ce^{4+}$ species with binding energies of 882.8, 889.4, 898.6, 901.2, 907.6 and 916.9 eV and $Ce^{3+}$ species with binding energies of 884.8 and 903.1 eV [54][55] coexist on the 5% Ce-15% In/SSZ-13 catalyst. Table 4 illustrates that the ratio of $Ce^{3+}/(Ce^{3+}+Ce^{4+})$ reaches 28.04%. The presence of $Ce^{3+}$ species results in the formation of a certain number of oxygen vacancies, and as a consequence, the $O_a$ concentration ($O^-$ and $O_2^-$) is increased via Eqs. (6)-(7) [56][57][58].

$$1/2O_2 + Ce^{3+} - \Delta \leftrightarrow Ce^{4+} - O^- \quad (\Delta\text{: oxygen vacancy}) \qquad (6)$$

$$O_2 + Ce^{3+} - \Delta \leftrightarrow Ce^{4+} - O_2^- \quad (7)$$

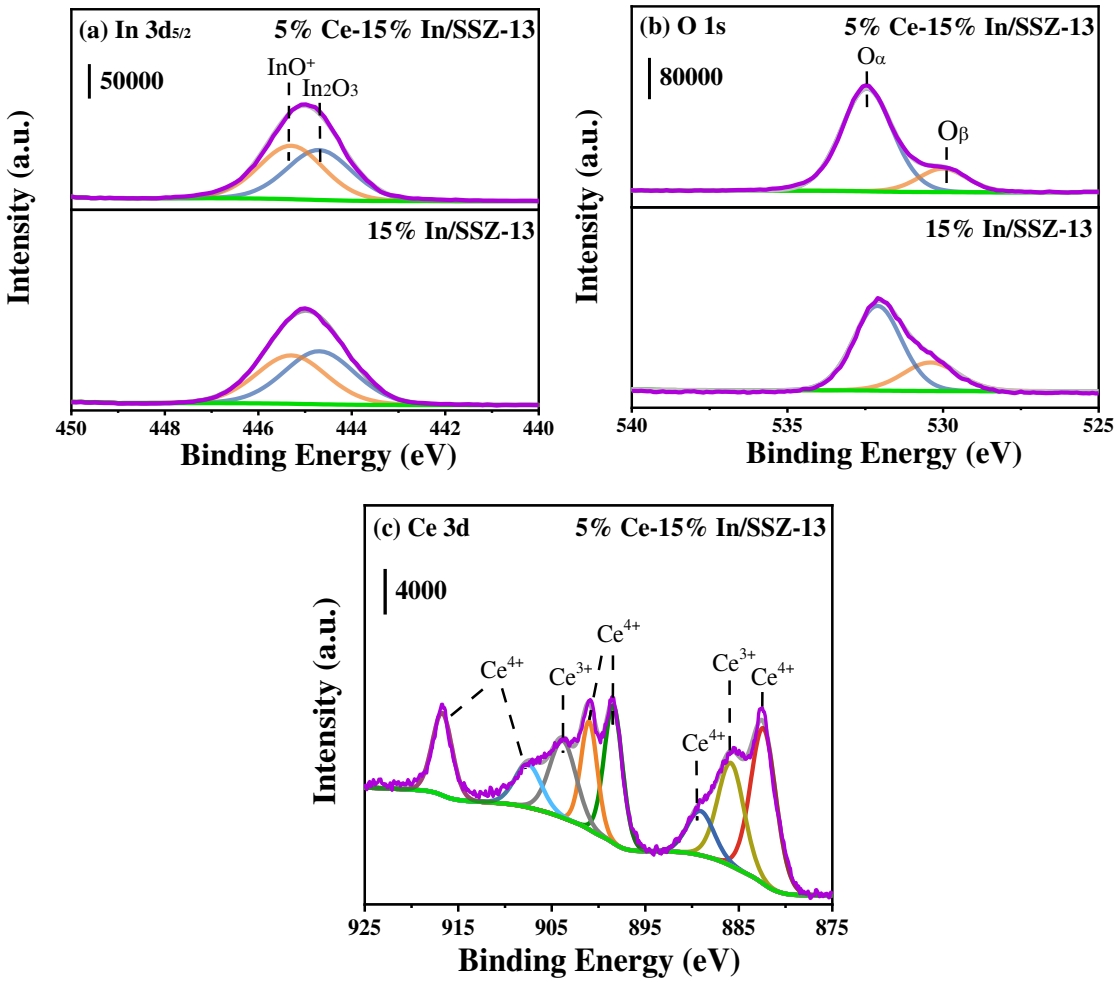


**Fig. 8.** XPS spectra of 15% In/SSZ-13 and 5% Ce-15% In/SSZ-13 catalysts. (a) In $3d_{5/2}$ region, (b) O 1s region, (c) Ce 3d region

**Table 4** Atomic ratios of different element chemical states

| Samples | 15% In/SSZ-13 | 5% Ce-15% In/SSZ-13 |
|---|---|---|
| $InO^+/(InO^+ + In_2O_3)$ | 47.61% | 51.38% |
| $Ce^{3+}/(Ce^{3+} + Ce^{4+})$ | - | 28.04% |
| $O_\alpha/(O_\alpha + O_\beta)$ | 72.2% | 82.2% |

### *3.4. Temperature-programmed desorption*

#### *3.4.1. NO-TPD and (NO+$O_2$)-TPD analysis*

The effects of Ce modification on the $NO_X$ adsorption were evaluated by TPD tests. The NO-TPD profiles in Fig. 9 (a) present a weak desorption peak at 130°C and a strong NO desorption peak at 330°C for both the 5% Ce-15% In/SSZ-13 and 15% In/SSZ-13 catalysts. Similarly, the ($NO+O_2$)-TPD profiles in Fig. 9 (b) also show two NO desorption peaks centered at 220°C and 330°C for these two catalyst samples. A very small amount of $N_2O$ and $NO_2$ are detected together with NO during the NO-TPD and (NO+O2)-TPD processes. In addition, it is obvious that the peak intensities of the 5% Ce-15% In/SSZ-13 catalyst are stronger than those of 15% In/SSZ-13 catalyst, which proposes that the Ce modification promotes the formation of NO adsorption species. This assertion is also supported by the data in Table 5, in which the 5% Ce-15% In/SSZ-13 catalyst has the larger total amount of NO desorption than the 5% In/SSZ-13 catalyst. For instance, the total amount of NO desorption for the former is 1.31 times that for the latter during the NO-TPD process.

Close inspection of Fig. 9 and Table 5 shows that the Ce modification can remarkably increase the increment of NO desorption amount in the presence of $O_2$. Table 5 manifests that after Ce modification, the total amount of NO desorption increases by 31.1% during the NO-TPD process, while the corresponding value is 107.8% during the ($NO+O_2$)-TPD process. This increment is because the Ce modification enhances the NO oxidation in the presence of $O_2$, which is confirmed by the results in Fig. 10. It is seen from Fig. 10 that the Ce modification substantially increases the conversions of NO to $NO_2$ in the presence of $O_2$. The enhancement of NO oxidation implies that more $NO_X$ species are adsorbed on the In sites [14][26], thus leading to an increase in NO desorption amount.

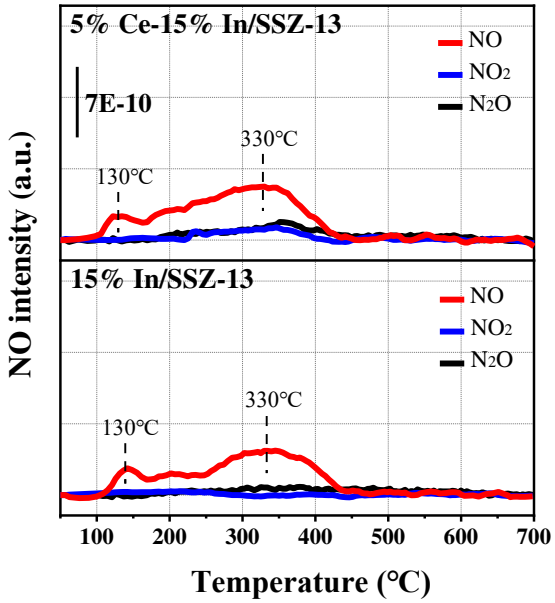


(a) NO-TPD

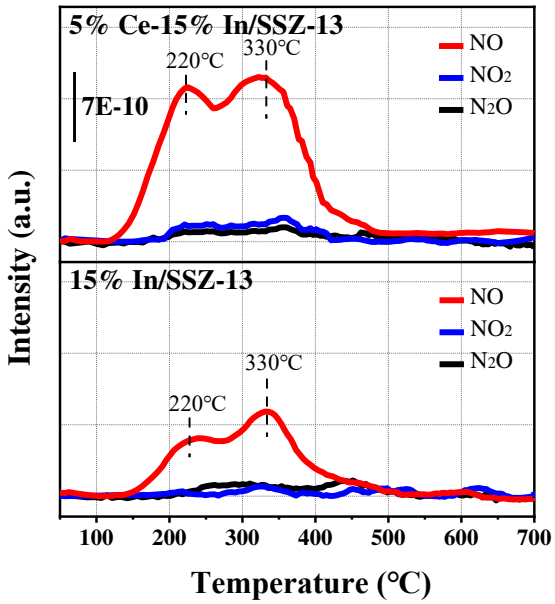


(b) (NO+$O_2$)-TPD

**Fig. 9.** NO-TPD and (NO+$O_2$)-TPD profiles over 15% In/SSZ-13 and 5% Ce-15% In/SSZ-13 catalysts.

**Table 5** NO desorption amount over the 15% In/SSZ-13 and 5% Ce-15% In/SSZ-13 catalysts

| | NO desorption amount (μmol/g) |
|---|---|

| Catalyst samples | NO-TPD | (NO+$O_2$)-TPD |
|---|---|---|
| 15% In/SSZ-13 | 120.6 | 169.5 |
| 5% Ce-15% In/SSZ-13 | 158.1 | 352.2 |

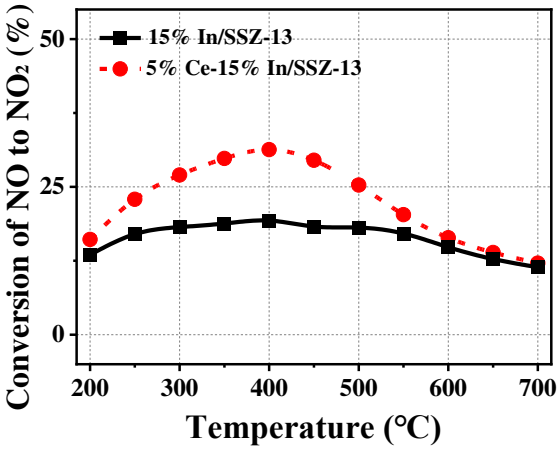


**Fig. 10.** Conversion of NO to $NO_2$ over 15% In/SSZ-13 and 5% Ce-15% In/SSZ-13 catalysts. Reaction condition: 1000 ppm NO and 8% $O_2$, 30000 $h^{-1}$ GHSV.

*3.4.2. $NH_3$-TPD analysis*

The effects of Ce modification on the catalyst acidity were evaluated by $NH_3$-TPD. The $NH_3$-TPD profiles in Fig. 11 shows two obvious desorption peaks for both the 15% In/SSZ-13 and 5% Ce-15% In/SSZ-13 catalysts. The low-temperature peak at 230°C is assigned to the $NH_3$ absorption on the Lewis acid sites formed by metal ions [59], and the high-temperature peak at 500°C corresponds to the strong absorption on Brønsted acid sites [60]. Notably, the 5% Ce-15% In/SSZ-13 catalyst has more Lewis acid sites than the 15% In/SSZ-13, which probably results from the introduction of Ce ions and the increase in $InO^+$. However, the Brønsted acid sites for the 5% Ce-15% In/SSZ-13 catalyst decrease because they are consumed in metal ion exchange process. In addition, a small peak appears at 310°C for the 5% Ce-15% In/SSZ-13 catalyst, which is attributed to the new Lewis acid sites

caused by the introduction of Ce ions.

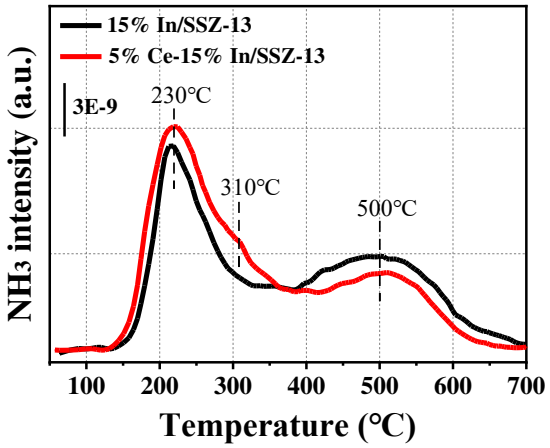


**Fig. 11.** $NH_3$-TPD profiles over 15% In/SSZ-13 and 5% Ce-15% In/SSZ-13 catalysts.

### *3.5. $H_2$-TPR analysis*

The redox ability of the catalyst samples was assessed using the $H_2$-TPR method. Figure 12 presents the $H_2$-TPR profiles of the 15% In/SSZ-13 and 5% Ce-15% In/SSZ-13 catalysts. The 15% In/SSZ-13 catalyst exhibits two $H_2$ consumption peaks at 300 and 400°C, assigning to the reduction of $InO^+$ and $In_2O_3$, respectively [17]. For the 5% Ce-15% In/SSZ-13 catalyst, the center of $InO^+$ characteristic peak moves to 290°C, and the intensity of $In_2O_3$ peak is slightly decreased. Because the reduction peak of $InO^+$ for the 5% Ce-15% In/SSZ-13 catalyst shifts toward lower temperature, the $InO^+$ species in proximity to the Ce are more readily reduced, and thus the reducibility of catalyst is enhanced. Compared with the 15% In/SSZ-13 catalyst, the $H_2$ consumption of the 5% Ce-15% In/SSZ-13 catalyst markedly increases, and the peak caused by the reduction of Ce species and $In_2O_3$ appears approximately at 480°C [61].

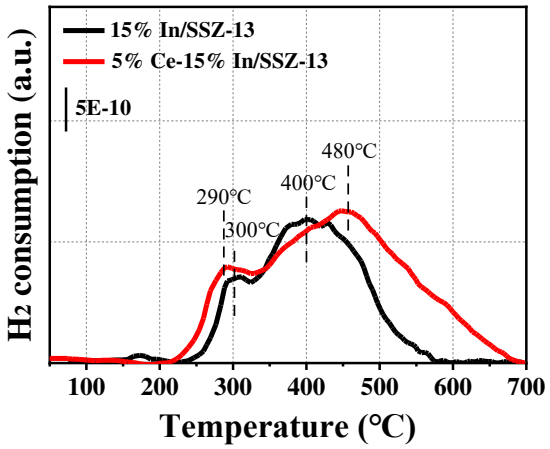


**Fig. 12.** $H_2$-TPR profiles over 15% In/SSZ-13 and 5% Ce-15% In/SSZ-13 catalysts.

### *3.6. $CH_4$ utilization efficiency*

In the present work, $CH_4$ acts as a reductant to involve in $NO_X$ SCR reaction via Eq. (5). However, a certain amount of $CH_4$ undergoes non-selective oxidation during trial, as evidenced by the NOx and $CH_4$ conversions in Figs. 1 and 2. Thus, the intense competition between $CH_4$ non-selective oxidation and SCR reaction is an important factor affecting $NO_X$ conversion [9][26]. Here, the CUE was introduced to evaluated this competition over15% In/SSZ-13 and 5% Ce-15% In/SSZ-13 catalysts, and the calculation method of CUE was provided in Section 2.2.

Figure 13 shows that the CUE values for both catalysts remain nearly 100% in the temperature region of <400°C and then substantially decrease with further increase in the temperature. This observation suggests that $CH_4$ non-selective oxidation occurs primarily in the high-temperature region, and the degree of $CH_4$ oxidation increases in response to the increase in temperature. Furthermore, it can be seen that the 5% Ce-15% In/SSZ-13 catalyst

has higher CUE value than the 15% In/SSZ-13 at the same temperatures. For instance, the CUE value of the former reaches 13.2% at 700°C, while the corresponding value of the latter is only 7.9%. In the preceding sections, the XPS analysis confirms that the In species in the catalyst exist in the form of $InO^+$ and $In_2O_3$, and the Ce modification decreases the ratio of $In_2O_3/(InO^+ + In_2O_3)$. In addition, the XRD results evidences that the Ce modification reduces the crystallinity and size of the $In_2O_3$ species. Large $In_2O_3$ agglomerates are inactive for the SCR reaction, but readily induce $CH_4$ non-selective oxidation [62]. Thus, the Ce introduction suppresses the non-selective oxidation of $CH_4$ in SCR reaction by inhibiting the formation and aggregation of $In_2O_3$, and as a consequence enables more $CH_4$ to be involved in the $NO_X$-SCR reaction, especially at high temperatures.

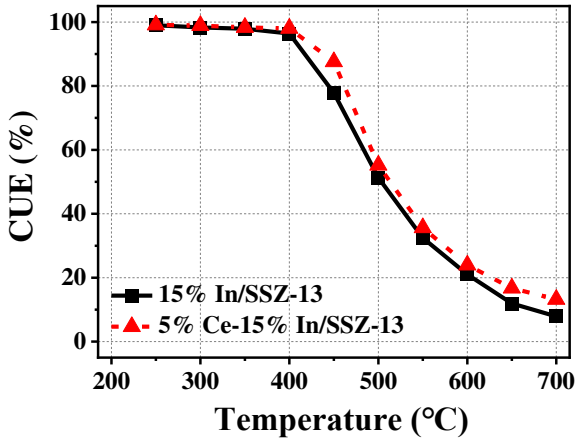


**Fig. 13.** $CH_4$ utilization efficiency (CUE) over the 15% In/SSZ-13 and 5% Ce-15% In/SSZ-13 catalysts in the $CH_4/NO_X$-SCR reaction.

## 5. Conclusions

The In/SSZ-13 catalysts were modified by Ce to further improve their catalytic performance for $CH_4$-SCR of $NO_X$ at high temperatures. After Ce modification, the

bimetallic 5% Ce-15% In/SSZ-13 catalyst possesses almost 100% $NO_X$ conversion at 450-620°C and more than 75% $NO_X$ conversion at 390-700°C, which are markedly superior to the monometallic 15% In/SSZ-13 catalyst. Furthermore, the Ce modification improves the water vapor tolerance of the catalyst sample, and the effect of water vapor on catalytic activity is reversible. Based on the catalyst characterizations and the $NO_X$ conversion and $CH_4$ oxidation measurements, the promotional mechanism of the Ce modification on the catalytic activity is identified:

1. Ce is present in two oxidation states, 3+ and 4+, on the catalyst surface. Because the $Ce^{3+}$ species provide more oxygen vacancies, the concentration of surface chemisorption oxygen species increases, and as a consequence promotes the oxidative activation of NO in the presence of $O_2$ during $CH_4/NO_X$-SCR reaction.

2. The Ce modification increases the relative amount of $InO^+$ species which serve as the main active sites for $CH_4$ activation. In addition, the Ce modification also increases the Lewis acid sites on catalyst surface.

3. The Ce modification tremendously promotes $NO_X$ adsorption on the catalyst surface, which is conducive to the enhancement of $NO_X$ conversions. Moreover, the Ce modification induces the $InO^+$ species to be readily reduced, and thus enhances the reducibility of the catalyst sample.

4. The $CH_4$ non-selective oxidation primarily occurs in the high-temperature region. The incorporation of Ce into In/SSZ-13 makes In species well dispersed on the catalyst surface, and thus suppresses the formation of bulk $In_2O_3$ species which are more active for $CH_4$ oxidation reaction.

## CRediT authorship contribution statement

**Chenxi Wang:** Conceptualization, Methodology, Investigation, Formal analysis, Data curation, Visualization, Writing - original draft. **Gang lv:** Funding acquisition, Resources, Investigation, Data curation. **Yunqiang Li:** Resources, Data curation. **Ye Liu:** Resources, Data curation. **Chonglin Song:** Conceptualization, Investigation, Project administration, Resources, Funding acquisition, Supervision, Writing - reviewing & editing.

## Declaration of competing interest

The authors declare that they have no known competing financial interests or personal relationships that could have appeared to influence the work reported in this paper.

## Acknowledgement

This study was supported by the National Natural Science Foundation of China (Grant number: 51921004).

## References

[1] Shen, X., Zhang, Y., Shen, T., Khajorntraidet, C., 2017. Spark advance self-optimization with knock probability threshold for lean-burn operation mode of SI engine. Energy. 122(3), 1-10.

[2] Naruke, M., Morie, K., Kouda, R., Sakaida, S., Tanaka, K., Konno, M., 2020. Investigation of fuel effects on the knock under lean burn conditions in a spark ignition engine. Fuel. 282, 118785.

[3] He, B.Q., Chen, X., Lin, C.L., Zhao, H., 2016. Combustion characteristics of a gasoline engine with

519 independent intake port injection and direct injection systems for n-butanol and gasoline. Energy
520 conversion & management. 124, 556-565.
521 [4] Kumar, G.S., Vishnuvarthan, M., Palanichamy, M., Murugesan, V., 2006. SBA-15 supported HPW:
522 Effective catalytic performance in the alkylation of phenol. Journal of Molecular Catalysis A:
523 Chemical. 260(1-2), 49-55.
524 [5] Gao, S., Wang, Y., Diao, X., Luo, G., Dai, Y., 2010. Effect of pore diameter and cross-linking method
525 on the immobilization efficiency of Candida rugosa lipase in SBA-15. Bioresource Technology.
526 101(11), 3830-3837.
527 [6] Tarach, K., Jabłońska, M., Pyra, K., Liebau, M., Góra-Marek, K., 2021. Effect of zeolite topology
528 on $NH_3$-SCR activity and stability of Cu-exchanged zeolites. Applied Catalysis B: Environmental.
529 284, 119752.
530 [7] Jabońska, M., 2022. Review of the application of Cu-containing SSZ-13 in $NH_3$-SCR-DeNOx and
531 NH3-SCO. RSC Advances. 12, 25240.
532 [8] Han, M., Jiao, Y., Zhou, C., Guo, Y., Guo, Y., Lu, G., Wang, L., Zhan W., 2019. Catalytic activity of
533 Cu-SSZ-13 prepared with different methods for NH3-SCR reaction. Rare Metals. 38(3), 24-34.
534 [9] González, J.M., Villa, A.L., 2021. High Temperature SCR Over Cu-SSZ-13 and Cu-SSZ-13 + Fe-
535 SSZ-13: Activity of $Cu^{2+}$ and $[CuOH]^+$ Sites and the Apparent Promoting Effect of Adding Fe into
536 Cu-SSZ-13 Catalyst. Catalysis Letters. 151, 3011-3019.
537 [10] Andana, T., Rappe, K.G., Nelson, N.C., 2022. Selective catalytic reduction of NOx with $NH_3$ over
538 Ce-Mn oxide and Cu-SSZ-13 composite catalysts – Low temperature enhancement. Applied
539 Catalysis B: Environmental. 316, 121522.
540 [11] Zhao, L., Qi, W., Wang, X., Su, X., 2020. Potentials of EGR and lean mixture for improving fuel

consumption and reducing the emissions of high-proportion butanol-gasoline engines at light load. Fuel. 266, 116959.

[12] Deng, B., Li, Q., Chen, Y., Li, M., Liu, A., Ran, J., Xu, Y., Liu, X., Fu, J., Feng, R., 2019. The effect of air/fuel ratio on the CO and NOx emissions for a twin-spark motorcycle gasoline engine under wide range of operating conditions. Energy. 169, 1202-1213.

[13] Prince, B., 2014. The Mechanisms of Methane C-h Activation and Oxy-insertion Via Small Transition Metal Complexes: a DFT Computational Investigation. Journal of the Mechanics & Physics of Solids. 65(5), 35-53.

[14] Ferenc, L., Hanna, E.S., Zoltán, P., Valyon, J., 2014. Mechanism of NO-SCR by methane over Co, H-ZSM-5 and Co, H-mordenite catalysts. Applied Catalysis B: Environmental. 150-151, 218-229.

[15] Ren, X., Tan, H., Jie, Q., Liu, J., 2020. DFT studies of the $CH_4$-SCR of NO on Fe-doped $ZnAl_2O_4$(100) surface under oxygen conditions. RSC Advances. 11, 927-933.

[16] Armor, J.N., 1995. Catalytic reduction of nitrogen oxides with methane in the presence of excess oxygen: A review. Catalysis Today. 26, 147-158.

[17] Pan, H., Jian, Y., Yu, Y., He, C., Shen, Z., Liu, H., 2017. Regeneration and sulfur poisoning behavior of In/H-BEA catalyst for NOx reduction by $CH_4$. Applied Surface Science. 401(15), 120-126.

[18] Li, Y., Wang, Q., Wang, D., Yan, X., 2019. NO-$CH_4$-SCR Over Core-Shell MnH-Zeolite Composites. Applied Science. 9, 1773.

[19] Lanas, J., Rojek, W., Shishido, T., Dzwigaj, D., 2012. Selective catalytic reduction of NO on single site FeSiBEA zeolite catalyst: Influence of the C1 and C2 reducing agents on the catalytic properties. Applied Catalysis B: Environmental. 123-124, 134-140.

[20] Chen, X., Zhu, A., Au, C.T., Shi, C., 2011. Enhanced Low-Temperature Activity of Ag-Promoted

563 Co-ZSM-5 for the $CH_4$-SCR of NO. Catalysis Letters. 141, 207-212.

564 [21] Mendes, A.N., Zholobenko, V.L., Thibault-Starzyk, F., Costa, P.D., Henriques, C., 2016. On the
565 enhancing effect of Ce in Pd-MOR catalysts for NOx $CH_4$-SCR: A structure-reactivity study.
566 Applied Catalysis B: Environmental. 195(15), 121-131.

567 [22] Sowade, T., Liese, T., Schmidt, C., Schutze, F.W., Yu, X., Berndt, H., Grunert, W., 2004. Relations
568 between structure and catalytic activity of Ce–In-ZSM-5 catalysts for the selective reduction of NO
569 by methane II. Interplay between the $CeO_2$ promoter and different indium sites. Journal of Catalysis.
570 225, 105-115.

571 [23] Li, Z., Flytzani-Stephanopoulos, M., 1999. On the Promotion of Ag-ZSM-5 by Cerium for the SCR
572 of NO by Methane. Journal of Catalysis. 182, 313-327.

573 [24] Liu, Z., Wang, K., Zhang, X., Wang, J., Cao, H., Gong, M., Chen, Y., 2009. Study on methane
574 selective catalytic reduction of NO on Pt/$Ce_{0.67}Zr_{0.33}O_2$ and its application. Journal of Natural Gas
575 Chemistry. 18, 66-70.

576 [25] Gao, E., Pan, H., Wang, L., Shi, Y., Chen, J., 2020. Identification of Main Active Sites and the Role
577 of $NO_2$ on NOx Reduction with $CH_4$ over In/BEA Catalyst: A Computational Study. Energies. 10(5),
578 572.

579 [26] Yang, J., Chang, Y., Dai, W., Wu, G., Guan, N., Li, L., 2018. Ru-In/H-SSZ-13 for the selective
580 reduction of nitric oxide by methane: Insights from temperature-programmed desorption studies.
581 Applied Catalysis B: Environmental. 236, 404-412.

582 [27] Blay, V., Louis, B., Miravalles, R., Yokoi, T., Peccatiello, K. A., Clough, M., Yilmaz, B., 2017.
583 Engineering Zeolites for Catalytic Cracking to Light Olefins. ACS Catalysis. 7, 6542– 6566.

584 [28] Usui, T., Liu, Z., Ibe, S., Zhu, J., Anand, C., Igarashi, H., Onaya, N., Sasaki, Y., Shiramata, Y.,

585 Kusamoto, T., Wakihara, T., 2018. Improve the Hydrothermal Stability of Cu-SSZ-13 Zeolite
586 Catalyst by Loading a Small Amount of Ce. ACS Catalysis. 8, 9165-9173.
587 [29] Tian, H., Ping, Y., Zhang, Y., Zhang, Z., Yang, X., 2021. Atomic layer deposition of silica to improve
588 the high-temperature hydrothermal stability of Cu-SSZ-13 for $NH_3$ SCR of NOx. Journal of
589 Hazardous Materials. 416, 126194.
590 [30] Shan, Y., Shan, W., Shi, X., Du, J., He, H., 2020. A comparative study of the activity and
591 hydrothermal stability of Al-rich Cu-SSZ-39 and Cu-SSZ-13. Applied Catalysis B: Environmental.
592 264, 118511.
593 [31] Charrad, R., Solt, H.E., Domjan, A., Ayari, F., Mhamdi, M., Valyon, J., Lonyi, F., 2020. Selective
594 catalytic reduction of NO by methane over Co, H-SSZ-13 catalysts: Types and catalytic functions
595 of active Co sites. Journal of Catalysis. 385, 87-102.
596 [32] Sulikowski, B., Lanas, J., Haber, A., Kubacka, A., Wloch, E., Olejniczak, Z., 1998. The synergetic
597 effect of cobalt and indium in ferrierite catalysts for selective catalytic reduction of nitric oxide with
598 methane. Chemical Communications. 214, 2755-2756.
599 [33] Eilertsen, E.A., Arstad, B., Svelle, S., 2012. Single parameter synthesis of high silica CHA zeolites
600 from fluoride media. Microporous and Mesoporous Materials. 153, 94-99.
601 [34] Yang, J., Chang, Y., Dai, W., Wu, G., Guan, N., Li, L., 2018. Bimetallic Cr-In/H-SSZ-13 for selective
602 catalytic reduction of nitric oxide by methane. Chinese Journal of Catalysis. 39(5), 1004-1011.
603 [35] Bin, F., Song, C., Lv, G., Song, J., Wu, S., Li, X., 2014. Selective catalytic reduction of nitric oxide
604 with ammonia over zirconium-doped copper/ZSM-5 catalysts. Applied Catalysis B: Environmental.
605 150-151, 532-543.
606 [36] Kwak, J.H., Tran, D., Burton, S.D., Szanyi, J., Lee, J.H., Peden, C.H.F., 2012. Effects of

hydrothermal aging on $NH_3$-SCR reaction over Cu/zeolites. Journal of Catalysis. 287, 203-209.

[37] Zhao, W., Shen, M., Zhu, Y., Wang, D., Li, X., 2021. Effect of mass ratio on micro-mesoporous Cu-SSZ-13/CeWTi composite catalysts for the selective catalytic reduction of NO with ammonia. RSC Advances. 11, 24883-24891.

[38] Aboul-Gheit, A.K., Aboul-Fotouh, S.M., Abdel-Hamid, S.M., Aboul-Gheit, N.A.K., 2006. Hydroconversion of cyclohexene using H-ZSM-5 zeolite catalysts promoted via hydrochlorination and/or platinum incorporation. Journal of Molecular Catalysis A: Chemical. 245(1-2), 167-177.

[39] Kwak, J. H., Varga, T., Peden, C. H. F., Gao, F., Hanson, J. C., Szanyi, J., 2014. Following the movement of cu ions in a SSZ-13 zeolite during dehydration, reduction and adsorption: A combined in situ TP-XRD, XANES/DRIFTS study. Journal of Catalysis. 314, 83-93.

[40] He, D., Wang, Z., Deng, D., Deng, S., Liu, L., 2020. Synthesis of Cu-SSZ-13 catalyst by using different silica sources for NO-SCR by $NH_3$. Molecular Catalysis. 484, 110738.

[41] Wang, X., Xu, Y., Qin, M., Zhao, Z., Fan, X., Li, Q., 2022. Insight into the effects of $Cu^{2+}$ ions and CuO species in Cu-SSZ-13 catalysts for selective catalytic reduction of NO by $NH_3$. Journal of Colloid and Interface Science. 622, 1-10.

[42] Villain, S., Cabane, J., Knauth, P., 1998. Solid state electrochemical characterisation of nanostructured silver prepared by cold-rolling and internal oxidation. Scripta Materialia. 38(6), 1003-1007.

[43] Shah, K.K., Nandi, M., Talukdar, A.K., 2015. Synthesis, characterization and catalytic activity of indium substituted nanocrystalline Mobil Five (MFI) zeolite. Materials Research Bulletin. 66, 101-108.

[44] Newalkar, B.L., Olanrewaju, J., Komarneni, S., 2011. Microwave-Hydrothermal Synthesis and

629 Characterization of Zirconium Substituted SBA-15 Mesoporous Silica. The Journal of Physical
630 Chemistry B. 105(35), 8356-8360.
631 [45] Serykh, A.I., Rozhdestvenskaya, N.N., 2015. Photoluminescence Properties of Indium-Exchanged
632 ZSM5 Zeolite. The Journal of Physical Chemistry C. 119, 17612-17618.
633 [46] Tang, B., Dai, W., Sun, X., Wu, G., Hunger, M., 2015. Incorporation of cerium atoms into Al-free
634 Beta zeolite framework for catalytic application. Chinese Journal of Catalysis. 36, 801-805.
635 [47] Kalita, B., Talukdar, A.K., 2012. Synthesis and characterization of Ce doped MFI zeolite. Materials
636 Chemistry & Physics. 133(2-3), 713-717.
637 [48] Gabrienko, A.A., Arzumanov, S.S., Moroz, I.B., Prosvirin, I.P., Toktarev, A.V., Wang, W., Stepanov,
638 A.G., 2014. Methane activation on In-modified ZSM-5: The state of indium in the zeolite and
639 pathways of methane transformation to surface species. The Journal of Physical Chemistry C.
640 118(15), 8034-8043.
641 [49] Shi, Y., Pu, J., Gao, L., Shan, S., 2021. Selective catalytic reduction of NOx with $NH_3$ and $CH_4$ over
642 zeolite supported indium-cerium bimetallic catalysts for lean-burn natural gas engines. Chemical
643 Engineering Journal. 403, 126394.
644 [50] Schwarz, H., 2011. Chemistry with methane: Concepts rather than recipes. Angewandte Chemie
645 International Edition. 50, 10096-10115.
646 [51] Zhao, W., Shen, M., Zhu, Y., Wang, D., Li, X., 2021. Effect of mass ratio on micro-mesoporous Cu-
647 SSZ-13/CeWTi composite catalysts for the selective catalytic reduction of NO with ammonia. RSC
648 Advances. 11, 24883-24891.
649 [52] Wu, Z., Jin, R., Liu, Y., Wang, H., 2008. Ceria modified MnOx/$TiO_2$ as a superior catalyst for NO
650 reduction with NH3 at low-temperature. Catalysis Communications. 9(13), 2217-2220.

[53] Kapteijn, F., Singoredjo, L., Andreini, A., Moulijn, J.A., 1994. Activity and selectivity of pure manganese oxides in the selective catalytic reduction of nitric oxide with ammonia. Applied Catalysis B: Environmental. 3(2-3), 173-189.

[54] Shi, Y., Tan, S., Wang, X., Li, M., Li, S., Li, W., 2016. Regeneration of sulfur-poisoned $CeO_2$ catalyst for $NH_3$-SCR of NOx. Catalysis Communications. 86(5), 67-71.

[55] Sartoretti, E., Novara, C., Chiodoni, A., Giorgis, F., Piumetti, M., Bensaid, S., Russo, N., Fino, D., 2022. Nanostructured ceria-based catalysts doped with La and Nd: How acidbase sites and redox properties determine the oxidation mechanisms. Catalysis Today. 390-391, 117-134.

[56] Zhang, R., Lu, K., Zong, L., Tong, S., Wang, X., Zhou, J., Lu, Z., Feng, G., 2017. Control synthesis of $CeO_2$ nanomaterials supported gold for catalytic oxidation of carbon monoxide. Molecular Catalysis. 442, 173-180.

[57] Grossale, A., Nova, I., Tronconi, E., Chatterjee, D., Weibel, M., 2008. The chemistry of the $NO/NO_2$-$NH_3$ "fast" SCR reaction over Fe-ZSM-5 investigated by transient reaction analysis. Journal of Catalysis. 256, 312-322.

[58] Cao, L., Chen, L., Wu, X., Ran, R., Xu, T., Chen, Z., Wen, D., 2018. TRA and DRIFTS studies of the fast SCR reaction over $CeO_2$ /$TiO_2$ catalyst at low temperatures. Applied Catalysis A: General. 557, 46-54.

[59] Wang, D., Zhang, L., Li, J., Kamasamudram, K., Epling, W.S., 2014. $NH_3$-SCR over Cu/SAPO-34-Zeolite acidity and Cu structure changes as a function of Cu loading. Catalysis Today. 231, 64-74.

[60] Liu, B., Yao, D., Wu, F., Hu, X., Li, Y., Wang, X., 2020. Ammonia dynamic modelling over Cu-SSZ-13 catalyst for NOx emission control in diesel vehicles. Reaction Chemistry & Engineering. 5(9), 1824-1832.

673 [61] Zhang, Z., Hu, G., Zhao, C., Wei, X., Dou, B., Liang, W., Bin, F., 2023. Insights into the reaction
674 mechanism of toluene oxidation by isotope dynamic experiment and the kinetics over MCeZr/TiO2
675 (M = Cu, Mn, Ni, Co and Fe) catalysts. Fuel. 341, 127760.
676 [62] Sowade, T., Schmidt, C., Schutze, F.W., Berndt, H., Grünert, W., 2003. Relations between structure
677 and catalytic activity of Ce-In-ZSM-5 catalysts for the selective reduction of NO by methane I. The
678 In-ZSM-5 system. Journal of Catalysis. 214, 100-112.
679